Cancer Letters 385 (2017) 75–86

Contents lists available at ScienceDirect

Cancer Letters

journal homepage: www.elsevier.com/locate/canlet

Original Article

Doxorubicin anti-tumor mechanisms include Hsp60 post-translational modifications leading to the Hsp60/p53 complex dissociation and instauration of replicative senescence

Antonella Marino Gammazza [a, b, *], Claudia Campanella [a, b], Rosario Barone [a, b], Celeste Caruso Bavisotto [a, b], Magdalena Gorska [c], Michal Wozniak [c], Francesco Carini [a], Francesco Cappello [a, b], Antonella D'Anneo [d], Marianna Lauricella [e], Giovanni Zummo [a], Everly Conway de Macario [f, g], Alberto J.L. Macario [b, f, g], Valentina Di Felice [a, b]

[a] Department of Experimental Biomedicine and Clinical Neurosciences, University of Palermo, Palermo, Italy
[b] Euro-Mediterranean Institute of Science and Technology, Palermo, Italy
[c] Department of Medical Chemistry, Medical University of Gdansk, Gdansk, Poland
[d] Department of Biological, Chemical and Pharmaceutical Sciences and Technologies, Laboratory of Biochemistry, University of Palermo, Palermo, Italy
[e] Department of Experimental Biomedicine and Clinical Neurosciences, Laboratory of Biochemistry, University of Palermo, Palermo, Italy
[f] Department of Microbiology and Immunology, School of Medicine, University of Maryland at Baltimore, Baltimore, MD, USA
[g] IMET, Columbus Center, Baltimore, MD, USA

ARTICLE INFO

Article history:
Received 29 July 2016
Received in revised form
26 October 2016
Accepted 28 October 2016

Keywords:
Doxorubicin
Hsp60
Acetylation
Ubiquitination
p53
Replicative senescence

ABSTRACT

The chaperone Hsp60 is pro-carcinogenic in certain tumor types by interfering with apoptosis and with tumor cell death. In these tumors, it is not yet known whether doxorubicin anti-tumor effects include a blockage of the pro-carcinogenic action of Hsp60. We found a doxorubicin dose-dependent viability reduction in a human lung mucoepidermoid cell line that was paralleled by the appearance of cell senescence markers. Concomitantly, intracellular Hsp60 levels decreased while its acetylation levels increased. The data suggest that Hsp60 acetylation interferes with the formation of the Hsp60/p53 complex and/or promote its dissociation, both causing an increase in the levels of free p53, which can then activate the p53-dependent pathway toward cell senescence. On the other hand, acetylated Hsp60 is ubiquitinated and degraded and, thus, the anti-apoptotic effect of the chaperonin is abolished with subsequent tumor cell death. Our findings could help in the elucidation of the molecular mechanisms by which doxorubicin counteracts carcinogenesis and, consequently, it would open new roads for the development of cancer treatment protocols targeting Hsp60.

Introduction

Replicative senescence (RS) or cellular senescence has been described as a state reached by normal mammalian fibroblasts cultured *in vitro* after a limited number of divisions [1]. In this state, senescent cells cannot divide and become un-responsive to growth signaling and resistant to apoptosis. Senescent cells show a flattened and enlarged shape and an increase in senescence-associated β-galactosidase (SA-β-gal) activity [2]. Cytoskeletal proteins may be involved in RS, for instance vimentin, since this protein is highly expressed in senescent fibroblasts [3].

Since cancer cells proliferate indefinitely, a requisite for their immortalization must be bypassing the physiological program that leads to RS. Abundant data support the notion that RS is a natural

Abbreviations: DMSO, dimethylsulfoxide; ELISA, enzyme linked immunosorbent assay; GAPDH, glyceraldehyde-3-phosphate dehydrogenase; GUSB, betaglucuronidase; HDAC, histone deacetylases; H2AX, H2A histone family member X; HPRT1, hypoxanthine phosphoribosyltransferase 1; Hsps, heat shock proteins; MTT, 3-(4,5-dimethylthiazol-2-yl)-2,3-diphenyltetrazolium bromide; OD, optical density; RS, replicative senescence; SA-β-gal, senescence-associated β-galactosidase; Sirt3, sirtuin 3; 17AAG, 17-(Allylamino)-17-demethoxygeldanamycin.

* Corresponding author. Department of Biomedicine and Clinical Neurosciences, Human Anatomy Section, Via del Vespro 129, 90127, Palermo, Italy.
E-mail address: antonella.marino@hotmail.it (A. Marino Gammazza).

http://dx.doi.org/10.1016/j.canlet.2016.10.045
0304-3835/

barrier against tumorigenesis [4,5]. Stress-induced premature senescence is a program executed by cells in response to chemotherapy, and RS induced by DNA-damaging anticancer drugs is one of the key determinants of successful chemotherapy [6].

Heat shock proteins (Hsps) are highly expressed in a variety of cancer cells and are essential to their survival contributing to tumor cell propagation, metastasis, and protection against apoptosis [7,8]. Several Hsps function as molecular chaperones for other proteins to prevent their aggregation after environmental stress, for example. Molecular chaperones participate in the response to anti-cancer drugs [9,10] and are intensively studied as therapeutic targets and as diagnostic and/or prognostic markers in many types of cancer, for example breast cancer, osteosarcomas [11], ovarian carcinoma [12], and pancreatic carcinoma [13]. As stated above, the senescence program seems to represent one of the major breaks on cancer emergence and it has been demonstrated that high levels of chaperones play an important role in suppressing the senescent program, keeping the p53 signaling under control and thus allowing cancer cells to proliferate [14]. In fact, specific down-regulation of Hsp70 leads to rapid senescence of various cancer cell lines [15], and human neuroblastoma cells displayed senescence-like characteristics after inhibition of Hsp90 with tanespimycin (17AAG) [16]. The mitochondrial chaperonin Hsp60 also named HSPD1 [17] was found in multiple subcellular sites and function in the folding and intracellular trafficking of many proteins [18,19]. Hsp60 has been found elevated in a large number of human carcinomas, which opens novel perspectives for cancer diagnosis and therapy targeting Hsp60 [20,21]. The chaperonin can activate the immune system [22] and can have both, pro-survival and pro-death functions, depending on tissue, cell type, and apoptosis inducers [23].

Senescence and apoptosis are alternative cell fates: in some cases apoptosis is a response to intense stress while senescence is a consequence of mild damage [4]. For example, doxorubicin, an anthracycline antitumor drug widely used in clinical chemotherapy, induces senescence at low doses and apoptosis at high doses in breast cancer cells and in neonatal rat cardiomyocytes [24,25,26]. Hsp60 over-expression suppressed doxorubicin-induced apoptosis in cardiomyocytes [27], and doxorubicin-induced apoptosis in HeLa cells triggering Hsp60 up-regulation [23]. To the best of our knowledge no data are available that would show a direct participation of Hsp60 in RS. Here we investigated if sub-apoptotic doses of doxorubicin have an impact on the tumor-favoring Hsp60 action and, thereby, produces anti-tumor effects via the induction of RS in a human lung mucoepidermoid cell line.

Materials and methods

Cell culture and treatment conditions

The human lung mucoepidermoid cell line NCI-H292 was obtained from the American Type Culture Collection. Cells were routinely propagated and maintained in Roswell Park Memorial Institute medium (RPMI-1640, Sigma Aldrich, Milan, Italy) with 10% heat-inactivated Fetal Calf Serum (FCS, Life Technology, Milan, Italy), supplemented with 2 mM glutamine, 100 U/ml penicillin, and 100 μg/ml streptomycin. The cell line was grown as monolayers attached to 25 cm^2 culture flasks and cultured at 37 °C, 5% CO_2 in a humidified incubator. Doxorubicin hydrochloride (Sigma Aldrich) was prepared as an 8 μM stock solution in sterile water, stored at −20 °C and freshly dissolved immediately before use. Working dilutions were made in sterile water and were added to the complete cell culture medium at the appropriate concentrations. Twenty-four hours after seeding, when the cells reached 70% confluency, the cultures were treated with a range of concentrations of doxorubicin (range 5–1280 nM) for 5 days and untreated cells (UT) were maintained as control. After that, the cell culture medium was replaced with fresh drug-free complete medium and cells were left to grow further for 24 h, before harvesting them for testing. Cells were routinely photographed before and after treatment to record morphological changes occurring in the cells, using an inverted light microscope equipped with phase contrast rings (LEICA DM-IRB, Leica Microsystem, Milan, Italy). Measurements of the area of the cell were done and evaluated using ImageJ Free software (NIH, Bethesda, MD).

MTT assay

The viability of NCI-H292 cells treated with doxorubicin was measured using 3-(4,5-dimethylthiazol-2-yl)-2,3-diphenyltetrazolium bromide (MTT) obtained from Sigma Aldrich. The assay was performed as described [28]. Briefly, 5×10^3 NCI-H292 cells were plated in 200 μl of complete medium per well in 96-well plates and treated with a series of doses of doxorubicin for 24, 48, or 72 h, or 5 days. MTT was dissolved in fresh medium and added to the cell cultures at a final concentration of 0.5 mg/ml. Following a 2 h incubation period, the converted dye was solubilized in 200 μl of dimethylsulfoxide (DMSO)/well and optical density (OD) was measured with a plate reader (Titertek Multiskan MCC/340, Flow Laboratories, Allschwil Switzerland) at 570 nm (630 nm as reference). Cell viability was expressed as the percentage of the OD value of inhibitor-treated cells compared with untreated controls, according to the following equation: Viability = (OD SAMPLE/OD CONTROL) × 100. Untreated cells were used as control and each experiment was carried out in triplicate.

Cell cycle analysis

Cells cultured in 25 cm^2 flasks were trypsinized and washed with phosphate buffered saline (PBS). The cells suspensions in PBS (1×10^6 cells/ml) were centrifuged and the supernatant was removed. To quantify DNA content, cells were fixed in absolute ethanol and resuspended in 1 ml of hypotonic buffer containing 0.1% Triton X-100, 0.1% sodium citrate, and 50 mg/ml propidium iodide (Sigma Aldrich) in propylene FACS tubes. After centrifugation at 1100 × g for 5 min and supernatant removal, the cells were resuspended again in 250 μl of hypotonic buffer and incubated in the dark at 23 °C for 15 min. Finally, 250 μl of RNAse A solution (10 μg/ml RNAse A in PBS) (Sigma Aldrich) was added to each tube following by an incubation of 15 min in the dark at 23 °C. After this treatment and the addition of 0.5 ml of PBS, the cells were analyzed by flow cytometry (FACScan; Becton-Dickinson, Milan, Italy). Percentages of cells in G0/G1, G2/M phases were determined, using APC32 acquiring software and analyzed by APC32 analysis software on a Coulter EPICS cytometer.

Senescence-associated beta-galactosidase (SA-β-gal) activity assay

SA-β-gal activity was detected using in situ β-gal staining kit (Agilent Technologies, Cernusco sul Naviglio, Milan, Italy) according to the manufacturer's protocols. Briefly, attached cells were fixed in a buffer including 2% formaldehyde/0.2% glutaraldehyde for 10 min at 23 °C. After removing the fixing solution from the wells, the cells were washed twice with PBS pH 7.6 and incubated with a freshly prepared staining solution (pH 6) containing X-gal (5-bromo-4 chloro-3-indolyl- β-gal-actopyranoside) overnight at 37 °C in a humidified incubator. Finally, coverslips were mounted with Vectamount A (Vector Laboratories, Peterborough, UK). The percentage of blue-stained cells in the total number of cells was determined by counting cells with a Leica DM 5000B light microscope.

Real-time quantitative PCR (qRT-PCR)

The qRT-PCR technique was performed as previously described [29]. Briefly, total cellular RNA was isolated from both control and treated cell cultures, using TRIzol®REAGENT (Sigma-Aldrich) and according to the manufacturer's instructions. RNA (50 ng) was retrotranscribed using the ImProm-II Reverse Transciptase Kit (Promega Corporation, Milan, Italy) to obtain cDNA, which was amplified using the StepOnePlus™ Real-Time PCR System (Thermo Scientific, Milan, Italy). qRT-PCR analysis was performed using GoTaq qPCR Master Mix (A6001, Promega). The mRNA levels were normalized to the levels obtained for hypoxanthine phosphoribosyltransferase 1 (HPRT1), for betaglucuronidase (GUSB), and for glyceraldehyde-3-phosphate dehydrogenase (GAPDH). The cDNA was amplified using the primers indicated in Table 1. cDNA was amplified using the Rotor-gene™ 6000 Real-Time PCR Machine (Qiagen GmbH, Hilden, Germany). Changes in the transcript level were calculated using the $2^{-\Delta\Delta CT}$ method [30].

Western blotting

Treated and untreated (control) NCI-H292 cells were harvested with 0.25% trypsin supplemented with 1 mM EDTA (LONZA, Basel, Switzerland) and centrifuged at 1100× g for 5 min at 4 °C. Pellets were washed twice in PBS and resuspended in 100 μl ice cold RIPA lysis buffer (0.3 M NaCl, 0.1% SDS, 25 mM HEPES pH 7.5, 1.5 mM $MgCl_2$, 0.2 mM EDTA, 1% Triton X-100, 0.5 mM DTT, 0.5% sodium deoxycholate) containing proteases and phosphatase inhibitors (0.1 mg/ml phenylmethyl sulfonyl fluoride, 20 mg/ml aprotinin, 20 mg/ml leupeptin, 10 mg/ml NaF, 1 mM DTT, 1 mM sodium orthovanadate, 20 mM ß-glycerol phosphate) to obtain lysates. Cell lysates were incubated for 30 min on ice then centrifuged at 13,000× g for 20 min at 4 °C. The Bradford assay was used to determine the total protein concentration. Equal amounts (40 μg) of total cellular proteins were resolved by SDS-PAGE and transferred to nitrocellulose membranes (Bio-Rad, Segrate, Milan, Italy). Equal protein loading was ascertained by Ponceau-S staining of blotted membranes. After 1 h incubation at 23 °C with a blocking solution, 5% milk in Tris buffered saline pH 7.6 (TBS) with 0.05% Tween 20 (Sigma-Aldrich) (T-TBS), membranes were incubated with primary antibodies (mouse anti-Hsp60, LK1 clone, Sigma Aldrich; mouse anti-vimentin, V9 clone, Santa Cruz Biotechnology, Heidelberg, Germany; mouse anti-

Table 1
Forward and reverse primers used for qRT-PCR.

Primer	Forward	Reverse
GUSB[a]	5'-ACCACCCCTACCACCTATATC-3'	5'-ATCCAGTAGTTCACCAGCCC-3'
GAPDH	5'-GAAACCCATCACCATCTTCC-3'	5'-TCCACGACATACTCAGCAC-3
HPRT1	5'-TGTCATGAAGGAGATGGGAG-3'	5'-ATCCAGCAGGTCAGCAAAG-3'
HSPD1 var1	5'-GAGTAGAGGCGGAGGGAG-3'	5'-AGTGAGATGAGGAGCCAGTA-3'

[a] GUSB, betaglucuronidase; GAPDH, glyceraldehyde-3-phosphate dehydrogenase; HPRT1, hypoxanthine phosphoribosyltransferase 1; HSPD1, Hsp60.

p53, DO-1 clone, Santa Cruz Biotechnology; rabbit anti-phosphorylated Histone H2AX (Ser 139; γH2AX), Santa Cruz Biotechnology; mouse anti-p21, clone DCS60, Cell Signaling Technology; mouse anti-β actin, AC-40 clone, Sigma-Aldrich). Membranes were then incubated with HRP-conjugated secondary antibody (ECL™ anti-mouse or anti-rabbit IgG HRP-conjugated whole antibody). The specific binding was detected using ECL (ECL™ Western Blotting detection, GE Healthcare Europe GmbH, Milan, Italy). The analysis of bands intensity was performed using ImageJ software.

Immunoprecipitation

Immunoprecipitation was performed as described previously [31] to detect protein complexes and post-translational modifications. Briefly, equal amounts of proteins (500 μg) from total cell lysates for each doxorubicin treatment were incubated with the primary anti-Hsp60 mouse monoclonal antibody overnight at 4 °C with gentle rotation. Antibody/protein complexes were then immunoprecipitated with antibodies linked to Sepharose A beads (GE Healthcare Europe GmbH). Nonspecifically bound proteins were removed by repeated washing with isotonic lysis buffer. Immunoprecipitated proteins were resolved by 10% SDS-PAGE using a primary antibody against acetylated lysine (mouse monoclonal anti-acetylated lysine, Cell Signaling, Pero, Milan, Italy), anti-ubiquitin primary antibody (mouse monoclonal anti-Ub, clone P4D1, Santa Cruz Biotechnology) and anti-p53 primary antibody. Each experiment was performed three times.

Immunofluorescence

Immunofluorescence was performed as described previously [32]. NCI-H292 cells were placed in 8-well microscope chamber slide at the density of 10,000 cells/well, cultured for 24 h and then treated with doxorubicin. Cells were fixed with ice-cold methanol for 30 min, washed in PBS pH 7.4, and then incubated with unmasking solution (trisodium citrate 10 mM, 0.05% Tween 20, pH 6) for 10 min at 23 °C. After rinsing twice with PBS, the cells were blocked with 3% (w/v) bovine serum albumin (BSA, Sigma Aldrich) in PBS for 30 min at 23 °C and incubated with the primary antibodies directed against Hsp60 and vimentin overnight at 4 °C. The day after, the cells were washed twice in PBS and were incubated with a fluorescent secondary antibody (mouse IgG antibody conjugated with FITC, Sigma-Aldrich) for 1 h at 23 °C in a moist chamber. The nuclei were counterstained with Hoechst 33342 (Sigma-Aldrich) for 15 min at 23 °C. Finally, the slides were covered with drops of PBS and mounted with coverslips. Imaging was immediately performed with a Leica DM5000 upright fluorescence microscope.

ELISA

Used culture medium was collected after the treatment with doxorubicin and ELISA was performed as previously described [33] to measure Hsp60, using a commercial Hsp60 (human) enzyme immunoassay (EIA) kit (Enzo Life Sciences, Vinci, Italy), according to the manufacturer's instructions. The Hsp60 protein standard was diluted in standard diluent to generate a standard curve with six points, ranging from 3.125 to 100 ng/ml. Then, 100 μl of prepared standards and samples was added in duplicate to wells of the immunoassay plate pre-coated with mouse monoclonal antibody specific for Hsp60 and incubated at 23 °C for 1 h and at 37 °C for 2 h. After diluting the primary and secondary antibodies according to the manufacturer's instructions, 100 μl of anti-Hsp60 goat polyclonal antibody was added to each well and incubated at 23 °C for 1 h and then at 37 °C for 1 h. Subsequently, 100 μl of horseradish peroxidase conjugate anti-goat IgG was added to the plate and incubated at 23 °C for 30 min followed by 100 μl of 3,3′,5,5′-tetramethylbenzidine substrate for 15 min in the dark. Finally, 100 μl of Stop Solution was added, and absorbance was measured at 450 nm with a microplate photometric reader (DV990BV4, GDV, Milan, Italy). Sample concentration was calculated by interpolating the sample measurement in the standard curve. The sensitivity of the human Hsp60 EIA kit was determined to be 3.125 ng/ml. Human Hsp60 EIA kit is specific for Hsp60 and the Hsp60 ELISA has been certified for the detection of human Hsp60.

Statistical analysis

The analysis was performed using the statistical software package GraphPad Prism4 (San Diego, CA). The data obtained were compared by the One-way ANOVA analysis of variance using Bonferroni post-hoc multiple comparisons. The data are expressed as means ± SD. The statistical significance threshold was fixed at $p < 0.05$.

Results

Inhibition of growth and morphological changes in lung cancer NCI-H292 cells exposed to doxorubicin

To determine the effects of doxorubicin on cell viability, NCI-H292 cells were cultured in RPMI supplemented with various concentrations of doxorubicin (range 5 to 1260 nM) at the beginning of the experiments (time 0) and were thereafter harvested at 24, 48, and 72 h, and at 5 days to determine viability and morphology. Cell growth was not inhibited after 24, 48, and 72 h (data not shown) but clear effects were observed after a five-day exposure to doxorubicin. A dose-dependent reduction of cell viability was evident as shown by MTT (Fig. 1). High doses of doxorubicin (640 and 1280 nM) decreased H292 cell viability inducing apoptotic cell death, as suggested by flow cytometry analysis (see later). On the basis of these results, three subapoptotic doses (20, 40, and 80 nM) were chosen to evaluate doxorubicin effect after 5 days of treatment. Morphological changes were already visible starting at 20 nM of doxorubicin. Cells showed a typical senescent phenotype appearing flattened and enlarged. In fact, the measure of their area increased concomitantly with the increase of doxorubicin doses (Supplementary Fig. S1, $p < 0.001$).

Doxorubicin induces replicative senescence in NCI-H292 cells

Flow cytometric examination of the cell cycle distribution of NCI-H292 cells showed a significant increase of cells with DNA content corresponding to G2/M at 80 nM of doxorubicin compared to the control and 20 nM ($p < 0.05$), whereas the cells

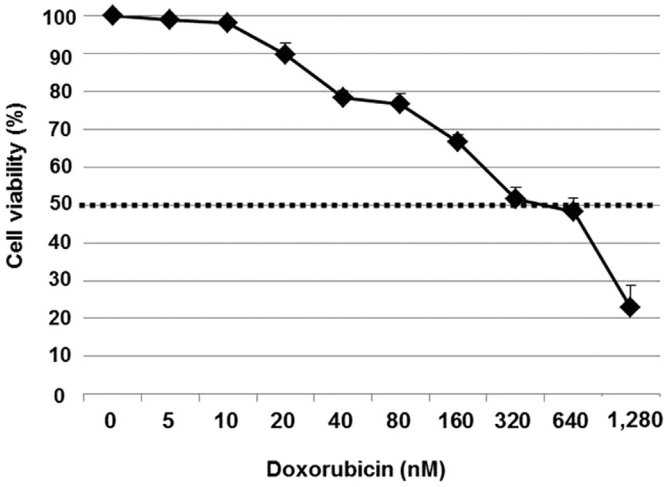

Fig. 1. Doxorubicin affects viability of NCI-H292 cells. The impact of doxorubicin was evaluated at 5 days of treatment at different concentrations by using MTT colorimetric assay. The viability data shown in the line chart pertain to day 5. After exposure to increasing concentrations (0–1280 nM) of doxorubicin, the cells showed a dose-dependent reduction of viability (growth 50% index: 480 nM).

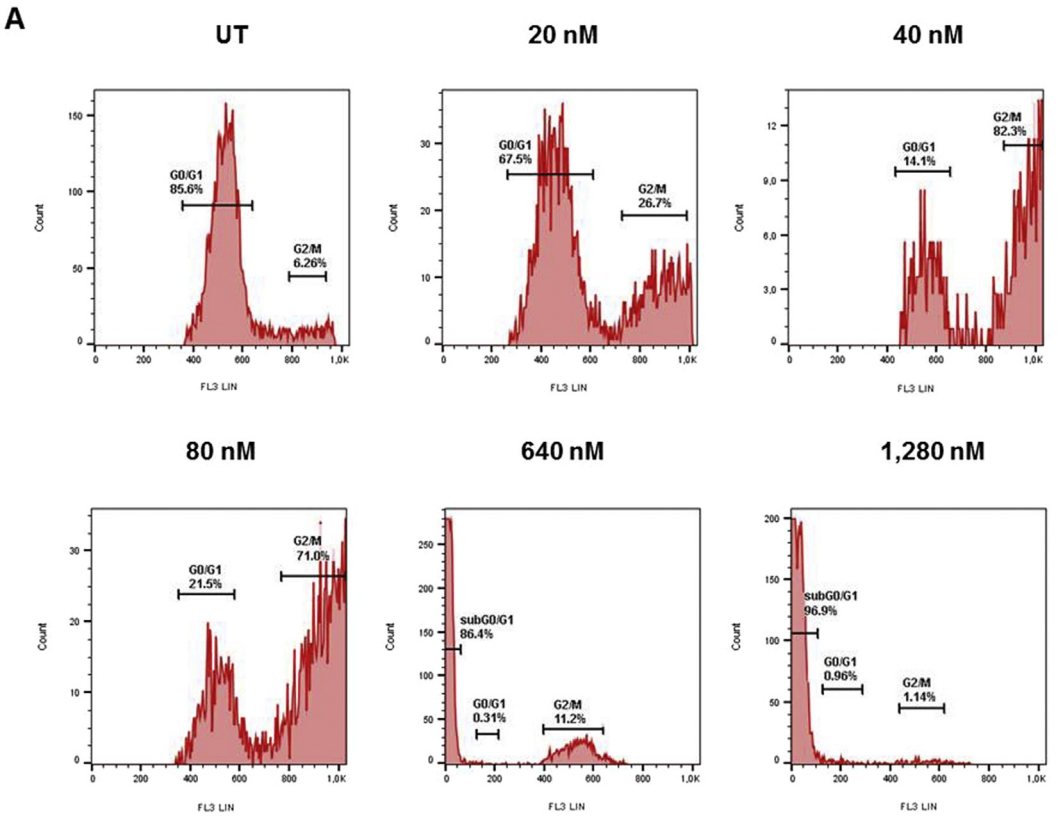
A
UT
G0/G1 85.6%
G2/M 6.26%
20 nM
G0/G1 67.5%
G2/M 26.7%
40 nM
G0/G1 14.1%
G2/M 82.3%
80 nM
G0/G1 21.5%
G2/M 71.0%
640 nM
subG0/G1 86.4%
G0/G1 0.31%
G2/M 11.2%
1,280 nM
subG0/G1 96.9%
G0/G1 0.96%
G2/M 1.14%
Count
FL3 LIN

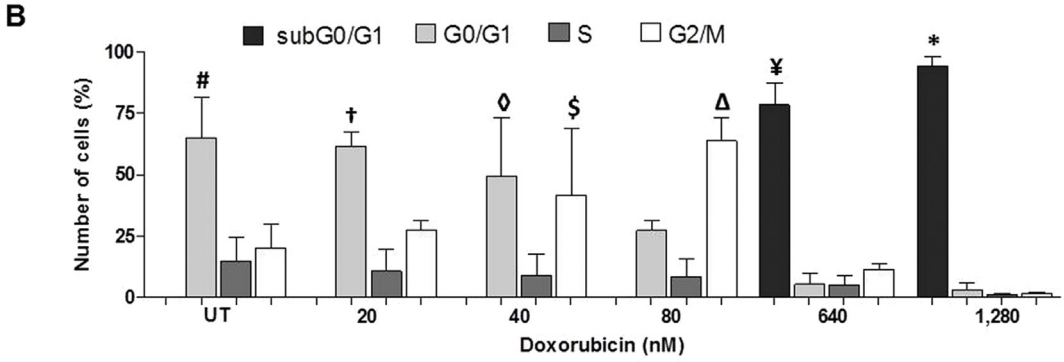
B
subG0/G1
G0/G1
S
G2/M
Number of cells (%)
Doxorubicin (nM)
UT
20
40
80
640
1,280

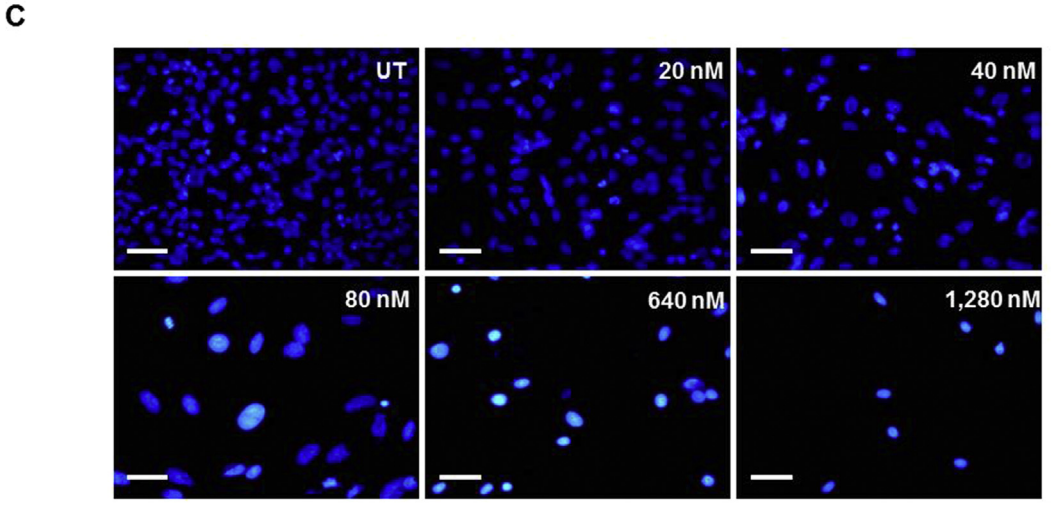
C
UT
20 nM
40 nM
80 nM
640 nM
1,280 nM

with DNA content corresponding to G0/G1 concurrently decreased ($p < 0.05$) (Fig. 2A–B). These results indicate that the drug induced cell cycle arrest. On the contrary, high doxorubicin doses (640 and 1280 nM) induced a significant increase in the number of cells with apoptotic features (sub G0/G1) corresponding to sub-diploid DNA content compared to all other conditions ($p < 0.001$) (Fig. 2A–B). In addition, the morphological analyses performed with fluorescence microscopy after staining with Hoechst showed that high doses of doxorubicin induced the appearance of highly condensed nuclei, which represent a typical apoptotic hallmark (Fig. 2C).

In order to determine whether the doxorubicin-induced cell cycle arrest is associated with RS in NCI-H292 cells, SA-β-gal activity and vimentin (which is known to be associated with cytoskeleton remodeling) were also determined. As shown in Fig. 3A, the number of β-gal-positive, i.e., senescent, cells was markedly increased in doxorubicin treated by comparison with untreated NCI-H292 cultures. Moreover, the percentage of β-gal-positive cells increased significantly with the dose of doxorubicin reaching the highest degree at 80 nM ($p < 0.01$) (Fig. 3B). Western blot analysis showed a significant increase in the level of the protein vimentin after treatment with 80 nM of doxorubicin compared with UT and 20 nM ($p < 0.05$; Fig. 4A–B). Fluorescence microscopic examination revealed that in control cells the vimentin network was subtle, relatively well organized, mainly composed of thin and short filaments uniformly distributed throughout the cytoplasm (Fig. 4C, upper left panel, UT). After the treatment, the cells appeared flattened and enlarged and a considerable heterogeneity in appearance and cytoplasmic location of filaments also occurred (Fig. 4C upper right panel, and both bottom panels). At 20 nM both unchanged cells and cells with increased volume were observed. These enlarged cells were more abundant at 40 and 80 nM of doxorubicin. Long filaments reached the peripheral regions of cells, but simultaneously few less-regularly arranged and dispersed fibers were observed in the vimentin network.

Effect of doxorubicin on p53, γH2AX, and p21 protein levels

In order to determine the effect of doxorubicin on p53 protein levels western blotting analysis was performed. As showed in Fig. 5A–B, doxorubicin at 20, 40 and 80 nM induced a significant increase of p53 protein levels to 1.7 fold compared to the untreated condition ($p < 0.01$). Since p53 can be activated in response to DNA damage, we analyzed the level of γH2AX, a histone H2A variant that becomes rapidly phosphorylated at serine 139 in response to DNA double-strand breaks and is a sensitive indicator of this DNA damage. By using a specific antibody directed against phosphorylated H2AX (Fig. 5C), we observed that 40 and 80 nM doxorubicin promoted a significant phosphorylation of H2AX at the Ser139 residue (γH2AX) compared to 20 nM and UT, favoring its activation (Fig. 5D, $p < 0.001$). Data reported in Fig. 5, panels C–E also demonstrated that the increase of p53 was accompanied by a significant up-elevation of p21 at 80 nM doxorubicin compared to all other conditions ($p < 0.001$). Moreover, p21 protein levels were significantly higher at 40 nM doxorubicin compared to UT and 20 nM ($p < 0.001$).

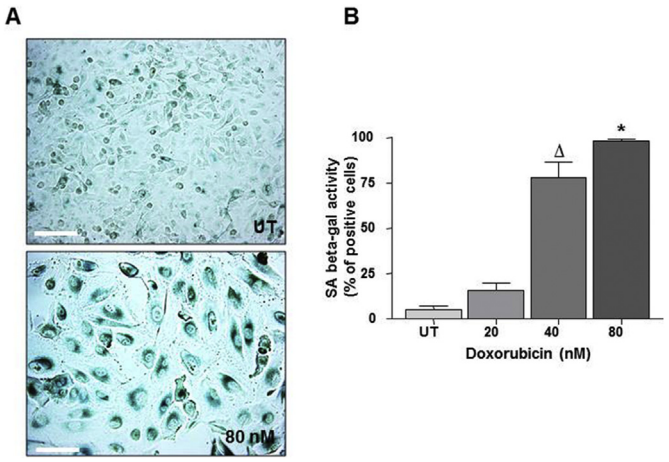

Fig. 3. SA-β-gal activity in NCI-H292 cells after treatment with doxorubicin. A: Representative images of senescence-associated β-galactosidase staining of untreated cells (UT), and of cells treated with 80 nM of doxorubicin for five days. The cells exhibited the typical blue staining. Bar = 100 μm (same for all panels). B: Histograms showing the percentage of cells positive for β-galactosidase staining. Results are representative of three independent experiments. * Different from UT, 20, and 40 nM $p < 0.01$; Δ Different from UT, and 20 nM $p < 0.001$. UT: untreated cells. (For interpretation of the references to color in this figure legend, the reader is referred to the web version of this article.)

Impact of doxorubicin on hsp60 gene expression and Hsp60 protein levels

To determine the effect of doxorubicin on *hsp60* gene expression qRT-PCR was applied. As shown in Fig. 6A, treatment with 40 and 80 nM of doxorubicin induced the increase of *hsp60* gene expression in NCI-H292 cells compared to 20 nM and non-treated cells ($p < 0.01$). Moreover, *hsp60* expression levels significantly increased at 80 nM doxorubicin compared to 40 nM dose ($p < 0.01$). On the other hand, the data obtained by Western blotting showed that Hsp60 protein levels were decreased down to 1.3 fold of the basal level in cells treated with 20 nM doxorubicin whereas its levels decreased to 1.8 and 2.5 at 40 and 80 nM doses respectively ($p < 0.05$) (Fig. 6B–C). Moreover, Hsp60 protein levels decreased at 80 nM doxorubicin compared to 20 nM dose ($p < 0.01$). Immunofluorescence confirmed that doxorubicin affected the Hsp60 protein levels and cell distribution (Fig. 6D).

Effect of doxorubicin on p53/Hsp60 complex and Hsp60 post-translational modifications and secretion

We next asked whether Hsp60 physically associated with p53, thus potentially limiting or abolishing its function. The interaction between Hsp60 and p53 in NCI-H292 cells was investigated using immunoprecipitation. A complex Hsp60/p53 was apparent in the untreated cells. The amount of p53 in the complex with Hsp60 significantly decreased after 40 and 80 nM doxorubicin compared to 20 nM and the untreated condition (Fig. 7A, top row of blots (a) and corresponding histogram, B; $p < 0.001$).

Fig. 2. Cycle distribution of NCI-H292 cells indicative of replicative senescence at sub-apoptotic doses. A: Representative flow cytometry histograms are shown for untreated (UT) cells, and for cells treated with 20, 40, 80, 640, and 1280 nM of doxorubicin. Cells were classified, according to DNA content, in the following categories: cells with DNA content corresponding to sub G0/G1, G0/G1, S, and G2/M. B: Cells with DNA content corresponding to G2/M significantly increased at 80 nM of doxorubicin compared to untreated cells, and to cells treated with 20, 640, or 1280 nM. DNA content corresponding to the S phase (S) was obtained as the difference between total DNA content (100) and the sum of DNA content corresponding to sub G0/G1, G2/M, and G0/G1. Cells with DNA content corresponding to sub G0/G1 significantly increased at 640 and 1280 nM compared to all other conditions. *Different from UT, 20, 40, 80, and 640 nM, $p < 0.001$; ¥Different from UT, 20, 40, and 80 nM, $p < 0.001$; #Different from 80, 640, and 1280 nM, $p < 0.05$; †Different from 80, 640, and 1280 nM, $p < 0.05$; ◊Different from 640, and 1280 nM, $p < 0.05$; ΔDifferent from UT, 20, 640, and 1280 nM, $p < 0,05$; $Different from 1280 nM, $p < 0.01$. C: Representative images showing the nuclei of the cells after staining with Hoechst. High doses of doxorubicin induced the appearance of highly condensed nuclei. Bar = 100 μm. UT: untreated cells.

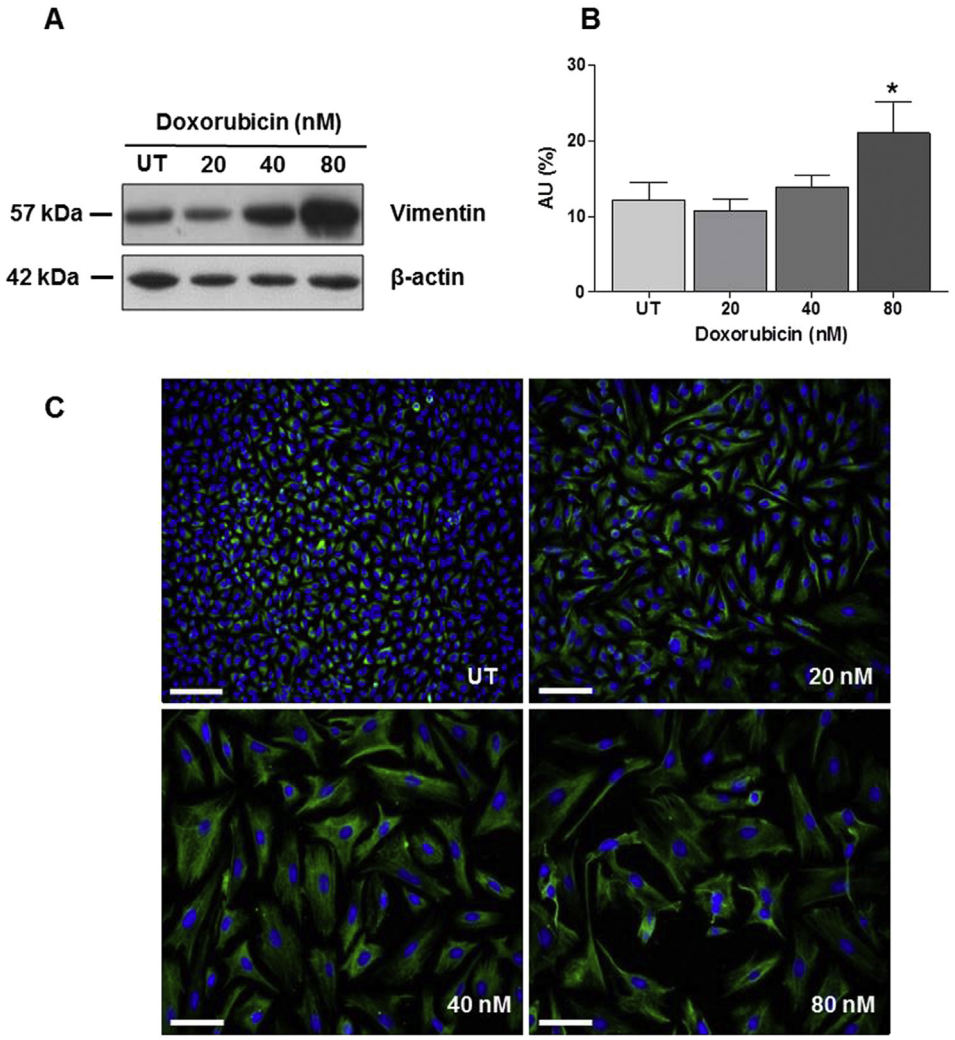

Fig. 4. Increase of vimentin levels and cytoskeleton remodeling in NCI-H292 cells after treatment with doxorubicin. A: Blots for vimentin showing its increase in cells treated with 40, or 80 nM of doxorubicin compared to untreated (UT) cells and to cells treated with 20 nM; β-actin was used as internal control. B. Ratio vimentin levels/β-actin levels as a measure of vimentin increase (mean ± SD). AU: arbitrary unit. *Different from UT, and 20 nM $p < 0.05$. C. Representative images showing vimentin increase and remodeling of the filaments. Nuclei were counterstained with Hoechst 33,342. Results are representative of three independent experiments. Bar = 100 μm (same for all panels).

In order to determine if doxorubicin induced post-translational modification of Hsp60, a double-labeled immunoprecipitation of Hsp60/acetylated lysine and Hsp60/ubiquitin was performed. The results showed that Hsp60 acetylation significantly increased at 40 and 80 nM doxorubicin compared to 20 nM and UT (Fig. 7A, second row of blots from the top (b) and corresponding histogram, C; $p < 0.05$), while the double-labeled immunoprecipitation of ubiquitin and the chaperonin, revealed that at 40 nM doxorubicin, Hsp60 was significantly ubiquitinated compared to other conditions (Fig. 7A third row of blots from the top (c) and corresponding histogram, D; $p < 0.01$).

Lastly, ELISA test was used to evaluate Hsp60 extracellular release. The results showed that Hsp60 release by treated cells into the extracellular medium was significantly decreased at 40 nM dose as compared to all other conditions ($p < 0.01$), while a borderline increase occurred at 80 nM compared to 20 nM (Fig. 7E; $p < 0.05$).

Discussion

Cellular senescence is a state of permanent cell cycle arrest that can be triggered by a variety of factors, including DNA damage, telomere shortening, and oxidative stress. Senescence limits the life span and proliferative capacity of cells, therefore the induction of this cellular process is nowadays an objective of anti-cancer treatment [34,35]. Senescence can offer an attractive therapeutic option if it can be restored in tumor cells, since many cancers cells retain the ability to senesce either spontaneously or in response to external stimuli [36]. However, the mechanisms for reactivating senescence in tumor cells are not well characterized and, therefore, the use of this therapeutic approach is underappreciated [37,38].

A promising field of research is the study of the role of Hsps in carcinogenesis, and of the possible applications of Hsp detection and quantification in tissues and biological fluids for cancer diagnosis, for assessing prognosis and monitoring disease progression, as well as for developing antitumor therapeutic strategies targeting Hsps [20]. Some key components of the senescence process are regulated by chaperones [19]. These proteins in cancer cells are believed to be involved in tumor progression and cell proliferation, differentiation, invasiveness, neoangiogenesis, metastasis, and immune system recognition [39,40] as well as in the development of chemotherapy resistance [41].

In our study, human-lung mucoepidermoid carcinoma cells were treated with a range of doses of doxorubicin. After treatment

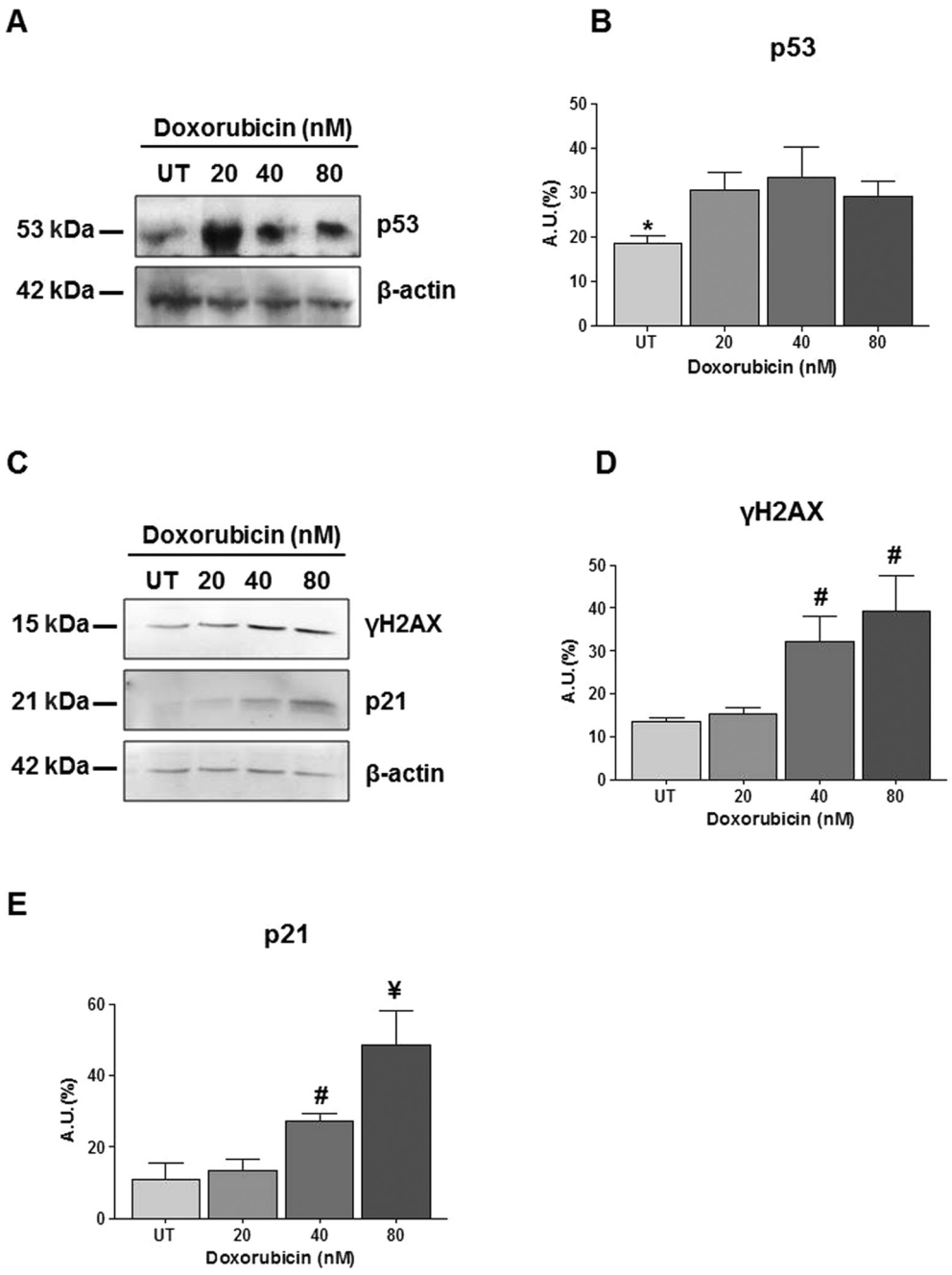

Fig. 5. Doxorubicin induced an increase in the levels of p53, γH2AX, and p21. A and C: Blots of p53, γH2AX, and p21 proteins in cells treated with 20, 40, or 80 nM, and untreated cells; β-actin was used as internal control. B, D, and E: Histograms representing the ratios p53/β-actin, γH2AX/β-actin, and p21/β-actin levels, respectively, calculated from the densitometric measurements of the blots in B and C, showing the increase in the three proteins in cells treated with doxorubicin (mean ± SD). AU, arbitrary unit; UT: untreated cells. *Different from 20, 40, and 80 nM $p < 0.01$; #Different from UT, and 20 nM $p < 0.001$; ¥Different from UT, 20, and 40 nM $p < 0.001$.

with 40 and 80 nM doxorubicin, the cells showed enlarged and flattened morphology, positivity to SA-β-gal activity, and cytoskeleton remodeling associated with an increase in the levels of vimentin, all typical indicators of RS, as also shown by others in other cell types [2,3]. Moreover, cell cycle analysis showed that the cells were in the G2/M phase at 80 nM, which is also in agreement with previous reports demonstrating that cellular senescence was associated with cell cycle arrest in the G2/M phase [42,43]. The mechanism by which different doses of doxorubicin may induce different stress-response programs is not well understood. The data obtained here demonstrated that doxorubicin induced the expression of the tumor suppressor protein p53. This is in agreement with previous studies reporting that the drug can intercalate DNA, generating reactive oxygen species, leading to a DNA damage-response mediated by p53 [26,44]. Coincident with these findings, our data provided evidence that doxorubicin was able to promote in lung mucoepidermoid NCI-H292 cells the activation of DNA damage response as suggested by the increase in γH2AX. In addition, other data have indicated the existence of a cause–effect relationship between the DNA damage response and cellular senescence [45]. In particular, it has been observed that some proteins involved in DNA damage response, including γH2AX, can localize at

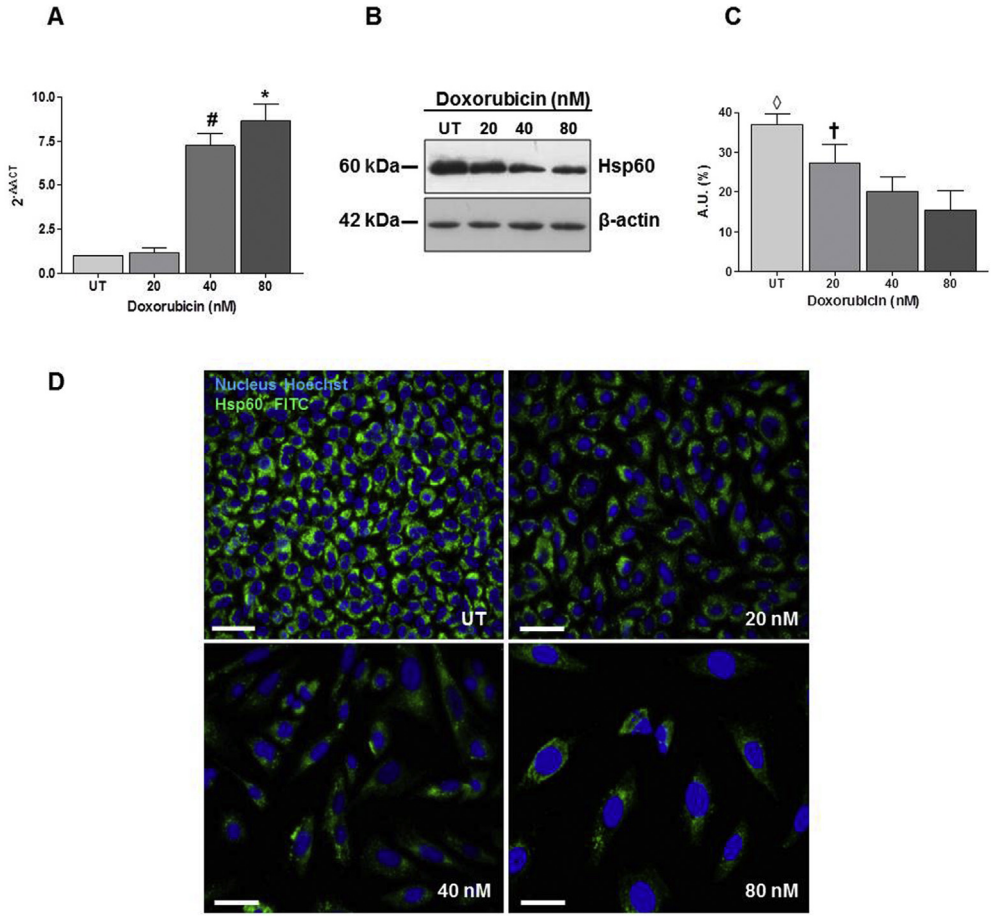

Fig. 6. *hsp60* gene expression and Hsp60 protein levels in NCI-H292 cells. A: Histograms representing qRT-PCR results that show changes in the transcript levels calculated using the $2^{-\Delta\Delta CT}$ method, which indicate that doxorubicin affected *hsp60* gene expression in NCI-H292 cells: namely, *hsp60* gene expression increased significantly in cells treated with 40 and 80 nM compared to untreated cells and to cells treated with 20 nM. B: Blots showing the decrease of Hsp60 protein levels in cells treated with 20, 40, or 80 nM of doxorubicin compared to untreated cells; β-actin was used as internal control. C: Histograms representing the ratio Hsp60 level/β-actin level that showHsp60 decrease at 40 and 80 nM compared to UT and 20 nM (mean ± SD). AU, arbitrary unit. D: Representative immunofluorescence images showing Hsp60 (green) decrease in cells treated with 40 or 80 nM of doxorubicin. Nuclei (blue) were counterstained with Hoechst 33,342. Bar = 100 μm (same for all panels). UT: untreated cells. $^{\#}$Different from UT, and 20 nM $p < 0.001$; *Different from UT, 20, and 40 nM $p < 0.01$; ◊Different from all other conditions $p < 0.05$; †Different from 80 nM $p < 0.01$. (For interpretation of the references to color in this figure legend, the reader is referred to the web version of this article.)

uncapped telomeres in the senescence-associated DNA damage [46]. The response activated by telomeric damage has been considered a potential inducer of senescence or cell death [47]. Moreover, our results showed an up-regulation of p21 after doxorubicin treatment, a transcriptional target of p53 which is involved in the induction of senescence [48].

Beyond the classical pathways involved in RS, here we provide experimental data demonstrating that treatment with doxorubicin inhibits the growth of a lung-cancer cell line via the induction of RS, which is accompanied by decreased levels of intracellular Hsp60. An increase of Hsp60 levels has been found correlated with the normal-to-dysplasia-to-carcinoma transitions in various anatomical sites [40] and with cell cycle progression [49]. Moreover, immunopositivity for Hsp60 was proposed as biomarker of bronchial carcinogenesis, considering that the levels of the chaperonin significantly correlated with the prognosis of lung adenocarcinoma [50]. Various data have revealed the need for Hsp60 by some types of tumor cells for their survival and growth. For example, elevated levels of this chaperonin in tumor cells have been linked to the ability to survive apoptotic stimuli, loss of RS, uncontrolled proliferation, and neoplastic transformation [51]. In our experimental model, decreased levels of Hsp60 were associated with appearance of senescence features and tumor-cell growth arrest, which coincided with Hsp60 modification such as hyperacetylation and ubiquitination. Hyperacetylation of Hsp60 can be due to the inhibition of sirtuins in line with observations by others who demonstrated that doxorubicin induced senescence in human dermal fibroblasts via down-regulation of both Sirtuin 1 and 2 [52]. Hyperacetylated Hsp60 could be tagged for the proteasome system, via ubiquitinization, which reached the highest degree a 40 nM, leading to a decrease of the intracellular levels of the chaperonin and the establishment of RS. This hypothesis is supported by the findings that in our model mRNA levels of Hsp60 where found elevated in contrast with the protein levels. The data obtained are consistent with *in vitro* experiments in which Hsp60 knockdown and inhibition of its expression by short hairpin RNA plasmids stopped tumor cell proliferation [53,54].

Hsp60 is preeminently a protein-folding machine but it can also stimulate anti-apoptotic mechanisms involving sequestration of Bax-containing complexes thus favoring tumor cell survival [51,55]. However, it has been demonstrated that Hsp60 modified with O-linked N-acetylglucosamine (O-GlcNAcylation) in pancreatic β-cells, under hyperglycemic conditions, shows a decreased interaction with Bax leading to cell death [56]. Loss of Hsp60 functions in a

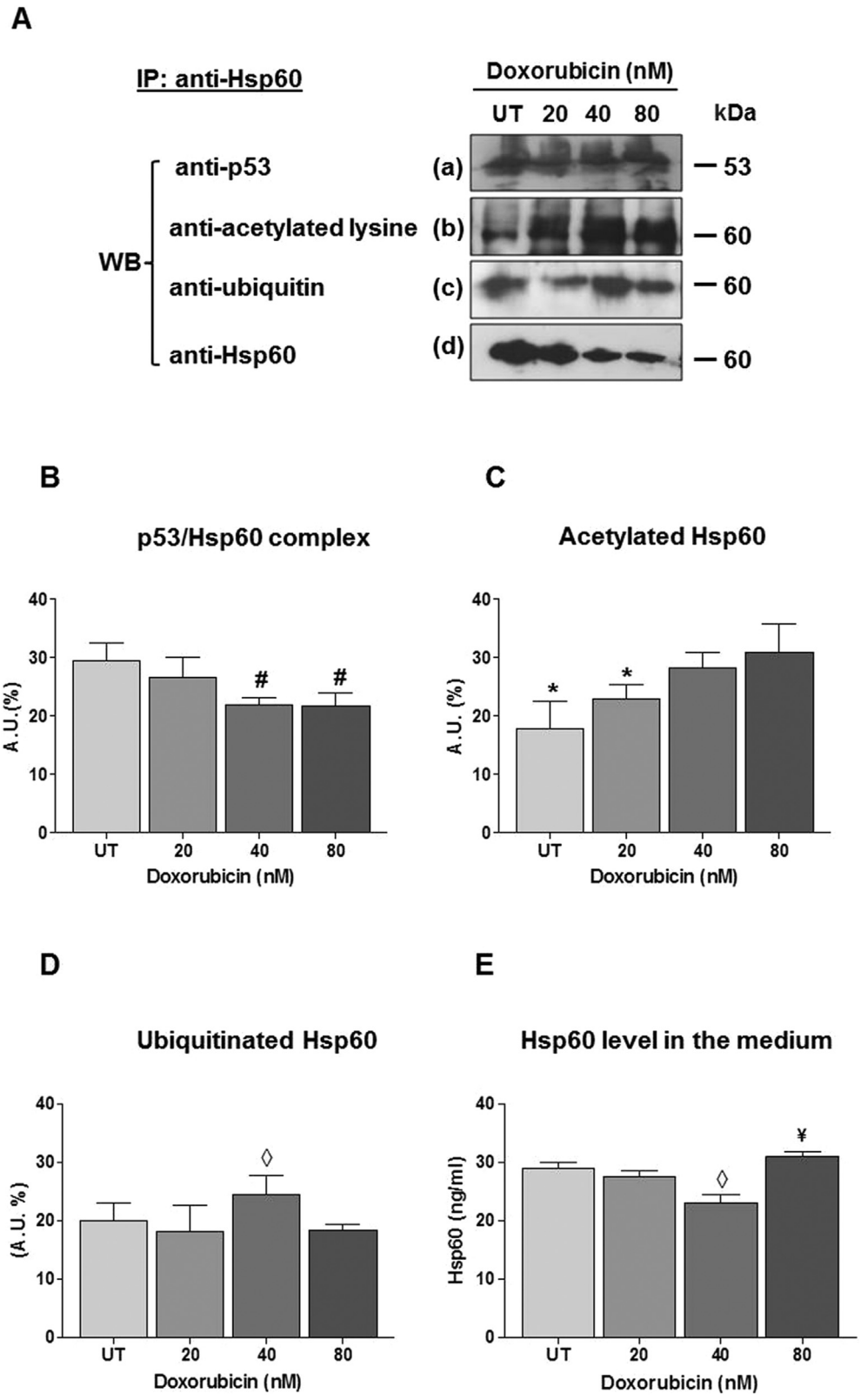

Fig. 7. Doxorubicin reduced p53/Hsp60 complex, and induced Hsp60 post-translational modification. A: Representative Western blots (WB) for immunoprecipitation experiments. Cell extracts from untreated cells and from cells treated with 20, 40, or 80 nM doxorubicin were prepared and protein complexes were immunoprecipitated using anti-Hsp60 antibody. Proteins were resolved by SDS-PAGE and identified using anti-p53 (a), anti-acetyl lysine (b), anti-ubiquitin (c), or anti-Hsp60 (d) antibody. B–D: Histograms representing densitometric measurements of the blots in A, showing: (*i*) the amount of p53 in the Hsp60/p53 complex significantly decreased in cells treated with 40 or 80 nM doxorubicin compared to UT and 20 nM (B); (*ii*) a dose-dependent increase in the levels of Hsp60 acetylation (C); and (*iii*) the ubiquitination of Hsp60 in cells treated with 40 nM doxorubicin (D). Histograms in panel E represent ELISA measurements and show a decrease in the levels of Hsp60 in the culture medium of cells treated with 40 nM of doxorubicin and a marginal increase of the chaperonin in the culture medium of cells treated with 80 nM. Results are representative of three independent experiments. AU, arbitrary unit; UT: untreated cells. $^{\#}$Different from UT, and 20 nM $p < 0.001$; *Different from 40, and 80 nM $p < 0.05$; ◊Different from all other conditions $p < 0.01$; $^{¥}$Different from 20 nM $p < 0.05$.

cancer cell, probably as a consequence of hyperacetylation for example after doxorubicin treatment, could lead to proteotoxic stress ultimately resulting in the switch of pro-survival signaling to cell-proliferation arrest. Our results are consistent with previous data demonstrating that hyperacetylation of Hsp60 was associated with anticancer activity of geldanamycin in osteosarcoma derived cells [32]. Hsp60 is one of the proteins that undergo acetylation in U2OS OS cells with sirtuin 3 (Sirt3) knockout [57]. Treatment with Histone Deacetylases (HDAC) inhibitors causes hyperacetylation of Hsp90, Hsp70, and Hsp40 and impairs their functioning. HDAC inhibitor-mediated deregulation of chaperone function, in turn, deregulates protein homeostasis and induces protein misfolding and proteotoxic stress [58,59].

To play a role in DNA damage response, p53 must interact with the promoter of target genes, an action that can be negatively affected by the interaction with protein inhibitors, such as Hsp60. In our control cells, p53 co-immunoprecipitated with Hsp60 and the complex could be considered as a prerequisite for malignant progression [51,60]. Doxorubicin treatment also caused the decrease of p53 in the Hsp60/p53 complex favored probably by the Hsp60 lysine (K) acetylation. From a structural point of view, the Hsp60 molecule is composed of various functional modules (and three structural domains named apical, intermediate, and equatorial) with distinct roles. If any of these modules is altered by a mutation, post-translational modification, or by the binding of a specific chemical compound, its functions may be seriously disrupted. This might lead to failure of the entire molecule and loss of its biological functions. For example, the apical domain contains conserved segments for substrate binding sites presenting lysine residues [20]. These findings suggest that stress signals induced by doxorubicin, promote Hsp60 post-translational modifications leading to the disruption of Hsp60/p53 complex and the activation of RS probably via p53-p21 pathway (Fig. 8), similarly to what has previously been proposed [61]. In line with these observations, we demonstrated that doxorubicin treatment increased the level of p21, a key factor capable of orchestrating cellular senescence [62]. Moreover, the decrease of the intracellular levels of the chaperonin may lead to a decrease in its extracellular release. Extracellular chaperones contribute to the intercommunication between different cells, tissues, and organs, in normal as well as in pathological conditions [18,63].

Extracellular Hsps have been considered to be multifunctional messengers involved in intercellular signaling [64]. It has been established that Hsp60 is actively secreted by human tumor cells and, thus, have potential as useful cancer biomarkers properties [29,40]. Hsp60 can be released from cells in free, soluble form, possibly via Golgi participating in extracellular molecular interactions and cell signaling, acting as a paracrine factor when released into the medium [3,40]. We observed a decrease in the release of the chaperonin in the culture medium at 40 nM doxorubicin concomitantly with the intracellular decrease of the protein levels and post-traslational modification. Hsp60 extracellular level marginally increased at 80 nM doxorubicin reaching the basal level probably as a result of cell death. A decrease of extracellular Hsp60 could affect the communication between tumor cells, a phenomenon in which Hsp60 would participate and, thereby, modulate the anti-tumor immuneresponse [65,66].

An overview of the data supports the notion that Hsp60 can favor carcinogenesis in the cells we studied. Furthermore, our observations shed light on the molecular mechanism by which doxorubicin acts as antitumor agent, i.e., likely by lowering the levels of intracellular Hsp60 and possibly also by impairing its functioning through acetylation. It thus becomes clear that targeting Hsp60 to diminish its levels (or block its functions) must be included in anti-tumor treatment strategies directed against cancers with elevated intracellular levels of the chaperonin.

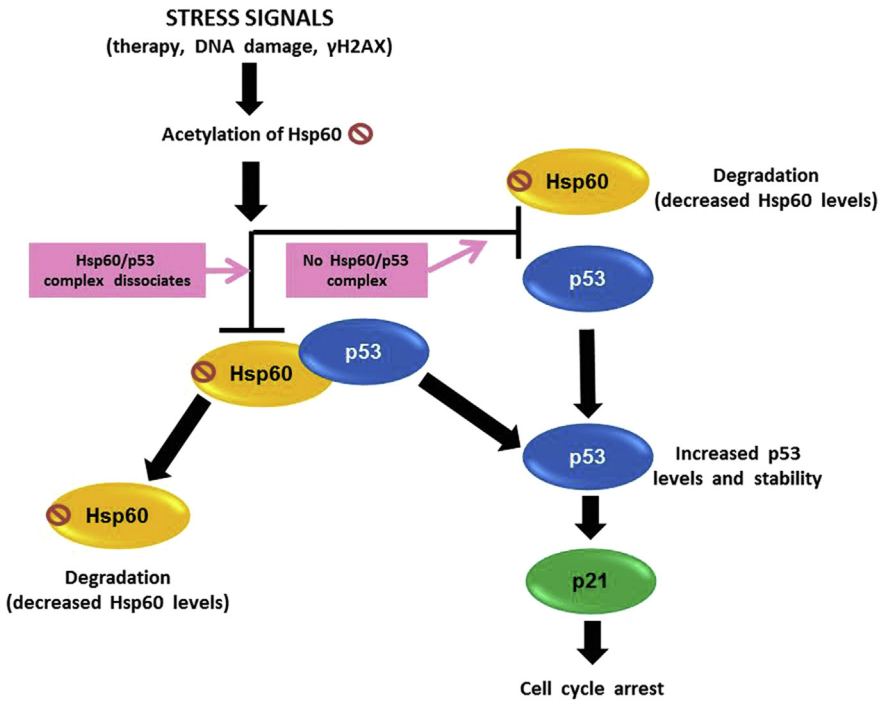

Fig. 8. Working hypothesis. In tumor cells there is normal Hsp60 free and Hsp60 bound to p53 (Hsp60/p53 complex). This allows tumor cell growth. Doxorubicin causes acetylation of Hsp60: it most likely acetylates the free Hsp60 (not bound to p53), but it may also cause acetylation of Hsp60 bound to p53 in the complex Hsp60/p53. The consequences are: (*i*) acetylated free Hsp60 cannot bind p53 and the complex Hsp60/p53 does not form; and (*ii*) acetylation of Hsp60 in the complex Hsp60/p53 causes dissociation of the complex with liberation of p53 (that goes on to induce replicative senescence via interaction with p21) and acetylated Hsp60. Acetylated Hsp60 is degraded with its consequent diminution inside the cell, which allows apoptosis to proceed. γH2AX, phosphorylated histone H2AX, considered a biomarker of DNA double-strand breaks.

Author contributions

A.M.G., C.C., and V.D.F. conceived the study and designed the experiments; A.M.G. wrote the manuscript; A.M.G., R.B., C.C.B, M.G., A.D, and M.L. performed experiments and analyzed data; M.W., F.C. A.D., M.L., G.Z., E.C. de M., and A.J.L.M. contributed to discussions, data processing and interpretation, and to manuscript writing; V.D.F., and F.C. provided funding. All authors reviewed the manuscript and approved the final version submitted.

Acknowledgments

This work was carried out using instruments provided by the Euro Mediterranean Institute of Science and Technology (IEMEST, Italy) and funded by the Italian National Operational Programme for Research and Competitiveness 2007–2013 grant (Project code: PONa3_00210, European Regional Development Fund). A.J.L.M. and E.C.de M. were partially supported by IMET; A.J.L.M. and F.C. were partially supported by IEMEST. This work was done under the umbrella of the agreement between IEMEST and the Institute of Marine and Environmental Technology (IMET; USA) signed in March 2012 (this is IMET contribution number IMET 16-184).

Conflicts of interest

None.

Appendix A. Supplementary data

Supplementary data related to this article can be found at http://dx.doi.org/10.1016/j.canlet.2016.10.045.

References

[1] M. Collado, M.A. Blasco, M. Serrano, Cellular senescence in cancer and aging, Cell 130 (2007) 223–233.
[2] G.P. Dimri, X. Lee, G. Basile, M. Acosta, G. Scott, C. Roskelley, et al., A biomarker that identifies senescent human cells in culture and in aging skin in vivo, Proc. Nat. Acad. Sci. U.S.A. 92 (1995) 9363–9367.
[3] K. Nishio, A. Inoue, Senescence-associated alterations of cytoskeleton: extraordinary production of vimentin that anchorscytoplasmic p53 in senescent human fibroblasts, Histochem Cell Biol. 123 (2005) 263–273.
[4] B.G. Childs, D.J. Baker, J.L. Kirkland, J. Campisi, J.M. Van Deursen, Senescence and apoptosis: dueling or complementary cell fates? EMBO Rep. 15 (2014) 1139–1153.
[5] A. Litwiniec, A. Grzanka, A. Helmin-Basa, L. Gackowska, D. Grzanka, Features of senescence and cell death induced by doxorubicin in A549 cells: organization and level of selected cytoskeletal proteins, J. Cancer Res. Clin. Oncol. 136 (2010) 717–736.
[6] I. Kikuchi, Y. Nakayama, T. Morinaga, Y. Fukumoto, N. Yamaguchi, A decrease in cyclin B1 levels leads to polyploidization in DNA damage-induced senescence, Cell Biol. Int. 34 (2010) 645–653.
[7] F. Rappa, C. Sciume, M. Lo Bello, C. Caruso Bavisotto, A. Marino Gammazza, R. Barone, et al., Comparative analysis of Hsp10 and Hsp90 expression in healthy mucosa and adenocarcinoma of the large bowel, Anticancer Res. 34 (2014) 4153–4159.
[8] M. Shevtsov, G. Multhoff, Heat shock protein-peptide and HSP-based immunotherapies for the treatment of cancer, Front. Immunol. 29 (7) (2016) 171.
[9] S.A. Harvey, K.O. Jensen, L.W. Elmore, S.E. Holt, Pharmacological approaches to defining the role of chaperones in aging and prostate cancer progression, Cell Stress Chaperones 7 (2002) 230–234.
[10] C. Zanini, G. Giribaldi, G. Mandili, F. Carta, N. Crescenzio, B. Bisaro, et al., Inhibition of heat shock proteins (HSP) expression by quercetin and differential doxorubicin sensitization in neuroblastoma and Ewing's sarcoma cell lines, J. Neurochem. 103 (2007) 1344–1354.
[11] D.R. Ciocca, S.K. Calderwood, Heat shock proteins in cancer: diagnostic, prognostic, predictive, and treatment implications, Cell Stress Chaperones 10 (2005) 86–103.
[12] B. Têtu, I. Popa, I. Bairati, S. L'Esperance, M. Bachvarova, M. Plante, et al., Immunohistochemical analysis of possible chemoresistance markers identified by micro-arrays on serous ovarian carcinomas, Mod. Pathol. 21 (2008) 1002–1010.
[13] M. Ogata, Z. Naito, S. Tanaka, Y. Moriyama, G. Asano, Overexpression and localization of heat-shock proteins mRNA in pancreatic carcinoma, J. Nippon. Med. Sch. 67 (2000) 177–185.
[14] M.Y. Sherman, V. Gabai, C. O'Callaghan, J. Yaglom, Molecular chaperones regulate p53 and suppress senescence programs, FEBS Lett. 581 (2007) 3711–3715.
[15] M. Rohde, M. Daugaard, M.H. Jensen, K. Helin, J. Nylandsted, M. Jäättelä, Members of the heat-shock protein 70 family promote cancer cell growth by distinct mechanisms, Genes Dev. 19 (2005) 570–582.
[16] U. Sarangi, K.R. Paithankar, J.U. Kumar, V. Subramaniam, A.S. Sreedhar, 17AAG treatment accelerates doxorubicin induced cellular senescence: Hsp90 interferes with enforced senescence of tumor cells, Drug Target Insights 6 (2012) 19–39.
[17] H.H. Kampinga, J. Hageman, M.J. Vos, H. Kubota, R.M. Tanguay, E.A. Bruford, et al., Guidelines for the nomenclature of the human heat shock proteins, Cell Stress Chaperones 14 (1) (2009) 105–111.
[18] F. Cappello, E. Conway de Macario, L. Marasà, G. Zummo, A.J.L. Macario, Hsp60 expression, new locations, functions and perspectives for cancer diagnosis and therapy, Cancer Biol. Ther. 7 (2008) 801–809.
[19] C.C. Deocaris, S.C. Kaul, R. Wadhwa, On the brotherhood of the mitochondrial chaperones mortalin and heat shock protein 60, Cell Stress Chaperones 11 (2006) 116–128.
[20] F. Cappello, A. Marino Gammazza, A. Palumbo Piccionello, C. Campanella, A. Pace, E. Conway de Macario, et al., Hsp60 chaperonopathies and chaperonotherapy: targets and agents, Expert Opin. Ther. Targets 18 (2014) 185–208.
[21] H. Tang, Y. Chen, X. Liu, S. Wang, Y. Lv, D. Wu, et al., Downregulation of HSP60 disrupts mitochondrial proteostasis to promote tumorigenesis and progression in clear cell renal cell carcinoma, Oncotarget 25 (2016) 38822–38834.
[22] A. Marino Gammazza, M. Rizzo, R. Citarrella, F. Rappa, C. Campanella, F. Bucchieri, et al., Elevated blood Hsp60, its structural similarities and cross-reactivity with thyroid molecules, and its presence on the plasma membrane of oncocytes point to the chaperonin as an immunopathogenic factor in Hashimoto's thyroiditis, Cell Stress Chaperones 19 (2013) 343–353.
[23] B.M. Gruber, J. Krzysztoń-Russjan, I. Bubko, E.L. Anuszewska, Possible role of HSP60 in synergistic action of anthracyclines and sulindac in HeLa cells, Acta Pol. Pharm. 67 (6) (2010) 620–624.
[24] P. Altieri, P. Spallarossa, C. Barisione, S. Garibaldi, A. Garuti, P. Fabbi, et al., Inhibition of doxorubicin-induced senescence by PPARdelta activation agonists in cardiac muscle cells: cooperation between PPARdelta and Bcl6, Plos One 7 (2012) e46126.
[25] Y.S. Song, B.Y. Lee, E.S. Hwang, Dinstinct ROS and biochemical profiles in cells undergoing DNA damage-induced senescence and apoptosis, Mech. Ageing Dev. 126 (2005) 580–590.
[26] P. Spallarossa, P. Altieri, C. Aloi, S. Garibaldi, C. Barisione, G. Ghigliotti, et al., Doxorubicin induces senescence or apoptosis in rat neonatal cardiomyocytes by regulating the expression levels of the telomere binding factors 1 and 2, Am. J. Physiol. Heart Circ. Physiol. 297 (2009) H2169–H2181.
[27] Y.X. Shan, T.J. Liu, H.F. Su, A. Samsamshariat, R. Mestril, P.H. Wang, Hsp10 and Hsp60 modulate Bcl-2 family and mitochondria apoptosis signaling induced by doxorubicin in cardiac muscle cells, J. Mol. Cell Cardiol. 35 (2003) 1135–1143.
[28] C. Campanella, A. D'Anneo, A.M. Gammazza, C. Caruso Bavisotto, R. Barone, S. Emanuele, et al., The histone deacetylase inhibitor SAHA induces HSP60 nitration and its extracellular release by exosomal vesicles in human lung-derived carcinoma cells, Oncotarget 20 (2015) 28849–28867.
[29] R. Barone, F. Macaluso, P. Catanese, A. Marino Gammazza, L. Rizzuto, P. Marozzi, et al., Endurance exercise and conjugated linoleic acid (CLA) supplementation up-regulate CYP17A1 and stimulate testosterone biosynthesis, Plos One 8 (2013) e79686.
[30] K.J. Livak, T.D. Schmittgen, Analysis of relative gene expression data using real-time quantitative PCR and the 2(-Delta Delta C(T)), Methods 25 (2001) 402–408.
[31] R. Barone, F. Rappa, F. Macaluso, C. Caruso Bavisotto, C. Sangiorgi, G. Di Paola, et al., Alcoholic liver disease: a mouse model reveals protection by lactobacillus fermentum, Clin. Transl. Gastroenterol. 7 (2016b) e138.
[32] M. Gorska, A. Marino Gammazza, M.A. Zmijewski, C. Campanella, F. Cappello, T. Wasiewicz, et al., Geldanamycin-induced osteosarcoma cell death is associated with hyperacetylation and loss of mitochondrial pool of heat shock protein 60 (hsp60), PLoS One 8 (2013) e71135.
[33] M. Rizzo, N. Abate, M. Chandalia, A.A. Rizvi, R.V. Giglio, D. Nikolic, et al., Liraglutide reduces oxidative stress and restores heme oxygenase-1 and ghrelin levels in patients with type 2 diabetes: a prospective pilot study, J. Clin. Endocrinol. Metab. 100 (2015) 603–606.
[34] M. Braig, S. Lee, C. Loddenkemper, C. Rudolph, A.H. Peters, B. Schlegelberger, et al., Oncogene-induced senescence as an initial barrier in lymphoma development, Nature 436 (2005) 660–665.
[35] X. Guo, W.M. Keyes, C. Papazoglu, J. Zuber, W. Li, S.W. Lowe, et al., TAp63 induces senescence and suppresses tumorigenesis in vivo, Nat. Cell Biol. 11 (2009) 1451–1457.
[36] Y. Kong, H. Cui, C. Ramkumar, H. Zhang, Regulation of senescence in cancer and aging, J. Aging Res. (2011) 963172.
[37] C.A. Schmitt, Senescence, apoptosis and therapy-cutting the lifelines of cancer, Nat. Rev. Cancer 3 (2003) 286–295.

[38] J.W. Shay, I.B. Roninson, Hallmarks of senescence in carcinogenesis and cancer therapy, Oncogene 23 (2004) 2919–2933.
[39] J. Ischia, A.I. So, The role of heat shock proteins in bladder cancer, Nat. Rev. Urol. 10 (7) (2013) 386–395.
[40] F. Rappa, F. Farina, G. Zummo, S. David, C. Campanella, F. Carini, et al., HSP-molecular chaperones in cancer biogenesis and tumor therapy: an overview, Anticancer Res. 32 (2012) 5139–5150.
[41] X. Wang, M. Chen, J. Zhou, X. Zhang, HSP27, 70 and 90, anti-apoptotic proteins, in clinical cancer therapy, Int. J. Oncol. 45 (2014) 18–30.
[42] V. Gire, V. Dulic, Senescence from G2 arrest, revisited, Cell Cycle 14 (2015) 297–304.
[43] M.B. Morelli, C. Amantini, M. Santoni, A. Soriani, M. Nabissi, C. Cardinali, et al., Axitinib induces DNA damage response leading to senescence, mitotic catastrophe, and increased NK cell recognition in human renal carcinoma cells, Oncotarget 6 (2015) 36245–36259.
[44] E.U. Kurz, P. Douglas, S.P. Lees-Miller, Doxorubicin activates ATM-dependent phosphorylation of multiple downstream targets in part through the generation of reactive oxygen species, J. Biol. Chem. 279 (2004) 53272–53281.
[45] J.H. Chen, C.N. Hales, S.E. Ozanne, DNA damage, cellular senescence and organismal ageing: causal or correlative? Nucleic Acids Res. 35 (2007) 7417–7428.
[46] H. Takai, A. Smogorzewska, T. de Lange, DNA damage foci at dysfunctional telomeres, Curr. Biol. 13 (2003) 1549–1556.
[47] F. d'Adda di Fagagna, P.M. Reaper, L. Clay-Farrace, H. Fiegler, P. Carr, T. von Zglinicki, et al., A DNA damage checkpoint response in telomere-initiated senescence, Nature 426 (2003) 194–198.
[48] I.B. Roninson, Oncogenic functions of tumour suppressor p21(Waf1/Cip1/Sdi1): association with cell senescence and tumour-promoting activities of stromal fibroblasts, Cancer Lett. 179 (2002) 1–14.
[49] Y.H. Lee, J.C. Lee, H.J. Moon, J.E. Jung, M. Sharma, B.H. Park, et al., Differential effect of oxidative stress on the apoptosis of early and late passage human diploid fibroblasts: implication of heat shock protein 60, Cell Biochem. Funct. 26 (2008) 502–508.
[50] X. Xu, W. Wang, W. Shao, W. Yin, H. Chen, Y. Qiu, et al., Heat shock protein-60 expression was significantly correlated with the prognosis of lung adenocarcinoma, J. Surg. Oncol. 104 (2011) 598–603.
[51] J.C. Ghosh, T. Dohi, B.H. Kang, D.C. Altieri, Hsp60 regulation of tumor cell apoptosis, J. Biol. Chem. 283 (2008) 5188–5194.
[52] K.E. Mehtap, A. Kilincli, O. Eren, Resveratrol induced premature senescence is associated with DNA damage mediated SIRT1 and SIRT2 down-regulation, Plos One 10 (2015) e124837.
[53] Z. Kaul, T. Yaguchi, S.C. Kaul, R. Wadhwa, Quantum dot-based protein imaging and functional significance of two mitochondrial chaperones in cellular senescence and carcinogenesis, Ann. N.Y. Acad. Sci. 1067 (2006) 469–473.
[54] R. Wadhwa, S. Takano, K. Kaur, S. Aida, T. Yaguchi, Z. Kaul, et al., Identification and characterization of molecular interactions between mortalin/mtHsp70 and HSP60, Biochem. J. 391 (2005) 185–190.
[55] A. Marino Gammazza, C.C. Bavisotto, R. Barone, E. Conway de Macario, A.J.L. Macario, Alzheimer's disease and molecular chaperones: current knowledge and the future of chaperonotherapy, Curr. Pharm. Des. 22 (2016) 4040–4049.
[56] H.S. Kim, E.M. Kim, J. Lee, W.H. Yang, T.Y. Park, Y.M. Kim, et al., Heat shock protein 60 modified with O-linked N-acetylglucosamine is involved in pancreatic beta-cell death under hyperglycemic conditions, FEBS Lett. 580 (2006) 2311–2316.
[57] E.M. Sol, S.A. Wagner, B.T. Weinert, A. Kumar, H.S. Kim, C.X. Deng, et al., Proteomic investigations of lysine acetylation identify diverse substrates of mitochondrial deacetylase Sirt3, Plos One 7 (2012) e50545.
[58] A.A. Khalil, N.F. Kabapy, S.F. Deraz, C. Smith, Heat shock proteins in oncology: diagnostic biomarkers or therapeutic targets? Biochim. Biophys. Acta (1816) 89–104, 2011.
[59] R. Rao, W. Fiskus, S. Ganguly, S. Kambhampati, K.N. Bhalla, HDAC inhibitors and chaperone function, Adv. Cancer Res. 116 (2012) 239–262.
[60] K.H. Vousden, Outcomes of p53 activation–spoilt for choice, J. Cell Sci. 119 (2006) 5015–5020.
[61] R. Mirzayans, B. Andrais, G. Hansen, D. Murray, Role of p16INK4A in replicative senescence and DNA damage-induced premature senescence in p53-deficient human cells, Biochem. Res. Int. (2012) 951574.
[62] B. Henderson, S.K. Calderwood, A.R. Coates, Caught with their PAMPs down? The extracellular signalling actions of molecular chaperones are not due to microbial contaminants, Cell Stress Chaperones 15 (2010) 123–141.
[63] A.M. Merendino, F. Bucchieri, C. Campanella, V. Marcianò, A. Ribbene, S. David, et al., Hsp60 is actively secreted by human tumor cells, Plos One 5 (2010) e9247.
[64] R. Barone, F. Macaluso, C. Sangiorgi, C. Campanella, A. Marino Gammazza, V. Moresi, et al., Skeletal muscle Heat shock protein 60 increases after endurance training and induces peroxisome proliferator-activated receptor gamma coactivator 1 α1 expression, Sci. Rep. 6 (2016a) 19781.
[65] S.K. Calderwood, M.A. Stevenson, A. Murshid, Heat shock proteins, autoimmunity, and cancer treatment, Autoimmun. Dis. 2012 (2012) 486069.
[66] C. Campanella, C. Caruso Bavisotto, A. Marino Gammazza, D. Nikolic, F. Rappa, S. David, et al., Exosomal heat shock proteins players in tumor cell-to-cell-communication, J. Circ. Biomark. 3 (2014) 1–10.